Development of amine-functionalized magnetic mesoporous carbon for dyes removal from single and binary: adsorption performance and mechanism

Fengping Hu, Min Wang*, Xiaoming Peng*, Hongling Dai, Yang Li

School of Civil Engineering and Architecture, East China Jiaotong University, Nanchang, 330013, Jiangxi Province, China,
Tel. (086) 0792 87046064; emails: wangminbetter@163.com (M.Wang), pengxiaoming70@126.com (X. Peng),
1325344563@qq.com (F. Hu), 12569825@qq.com (H. Dai), 33642673@qq.com (Y. Li)

ABSTRACT

Amine-functionalized magnetic mesoporous carbons (AFMMC) were prepared by a casting process using hard template, and ammonia gas and ferric salt as the nitrogen and iron source, which exhibited excellent adsorbents properties for the removal of anionic dye orange II (O II) or cationic dye methylene blue (MB) from aqueous solution. The AFMMC showed a higher adsorption capacity of two dyes than origin mesoporous carbon (MC), the improved adsorption capacity of AFMMC can be mainly attributed to the successfully introduction of the basic nitrogen-containing functional groups on the surface of mesoporous carbon. As isolated compounds and as a mixture of both of systems, equilibrium adsorption isotherms and kinetics were studied. During single dye solution system, the adsorption data of two dyes could be better described by the Langmuir model and pseudo-second-order model. Moreover, for AFMMC, the maximum adsorption capacities of 389.6 and 325.3 mg g^{-1} for O II and MB dyes in single dye solutions, respectively. The thermodynamic studies reveal that the adsorption of two dyes onto the MC and AFMMC were spontaneous and exothermic. The binary-component system was better described with Langmuir–Freundlich isotherm models. The results indicated that the presence of competitive adsorption between O II and MB dye occurred in binary systems, the maximum adsorption amount of O II or MB dye in two dyes binary-mixture systems is less than that of the single dye system. In addition, the removal ability of O II or MB dye after desorption not significantly decreased, demonstrating an excellent regeneration ability of AFMMC. The as-prepared AFMMC materials have the potential to be used for the efficient removal of organic pollutants.

Keywords: Amine-functionalized magnetic mesoporous carbon; Dye; Single and binary adsorption; Adsorption isotherms and kinetics; Regeneration

1. Introduction

Synthetic organic dye wastewater has emerged as one of the most common contaminants in the environment due to their extensive use in many industries, such as the textile, paper, plastic, food, printing, and cosmetics industries [1]. Many of these dyes and pigments are inert, toxic, and non-biodegradable when directly discharged into aquatic ecosystems through untreated waste. In addition, dyes and pigments result in colored effluent, which affects water transparency along with their high photolytic stabilities,

resulting in a reduction in sunlight penetration and oxygen gas solubility in water. The literature estimates that over 7×10^5 tons of dye wastewater are annually discharged into aquatic ecosystems [2]. Additionally, the discharge of intensely colored dye effluents and their degradation products into aquatic ecosystems causes serious mutagenic and carcinogenic problems to humans and other organisms [3].

Several treatment processes, including chemical oxidation [4], biodegradation [5], photocatalytic degradation [6], and adsorption [7], have been developed in recent decades for removing dyes from wastewater. Among these treatment

* Corresponding authors.

techniques, adsorption is the most conventional and is favorable for removing dyes owing to its simple design, ease of operation, and high toxic substance removal efficiency [8,9]. Some researchers have studied the production of activated carbon from bamboo [10], tires [11], mangosteen peel [12], sawdust [13], oil palm biomass [14], and sludge [15]. Mesoporous carbon, a promising and effective carbon material adsorbent, has already received much attention in for the large-scale removal of various dyes from aqueous solutions owing to its unique physical structure and large pore size, which would favor the adsorption of dyes with different molecular structures [16,17].

Some recent studies have focused on including functional groups (such as carboxyl, hydroxyl, and amine) on the surfaces of adsorbents to significantly improve the capacity and efficiency of adsorbent materials. As the performance of an adsorbent is influenced by its surface chemical structure in most applications, several treatments have been developed to modify its properties [18]. Therefore, it is important to determine the functional surface groups of the prepared adsorbents. Amine-grafted adsorbents have recently emerged as a promising technology that involves the introduction of groups to the solid's surface, which can effectively increase the adsorption capacity for organic or inorganic contaminants from an aqueous solution [16].

However, such technologies are difficult to apply in some cases as they do not easily recover or separate powdered mesoporous carbon from the mixture after the adsorption stage [19]. Various magnetic nanoparticles with novel physical and chemical properties have received much attention as they can easily be recycled from an aqueous solution using a magnetic field. Therefore, magnetized nanomaterials have also received widespread attention due to their safety, excellent dispersal in an aqueous solution, low cost, and ability to regenerate, as well as their magnetic recoverability [20,21].

The aim of this study is to fabricate a recyclable and regenerable magnetic mesoporous carbon material by modifying it with ammonia gas and further coating it with iron nitrate by co-precipitation, and to then use it as an adsorbent for removing anionic (OII) and cationic dye (MB) from an aqueous solution. Mesoporous nanocomposites could solve the problem that nanomaterials are not easily regenerated and recycled after use. In addition, the modified adsorbent exhibited a better adsorption capacity for the two dyes than the untreated mesoporous carbon. This study focuses on the single and binary adsorption abilities of the two dyes. The effects of pH, ionic concentration, and temperature were evaluated to ascertain the single-component adsorption performance. Thermodynamic data for adsorption at different temperatures were also calculated to further understand the adsorption process. In addition, batch experiments were conducted to explore the materials ability to adsorb an O II-MB

mixture from an aqueous solution. The kinetic models and single- and multi-component isotherms were estimated to explain the binary adsorption mechanism. In addition, the reusability and recyclability of the amine-functionalized magnetic mesoporous carbons (AFMMC) were assessed.

2. Materials and methods

2.1. Materials

Triblock copolymer $EO_{20}PO_{70}EO_{20}$ (Pluronic P123), tetraethyl orthosilicate (TEOS, 98%), furfuryl alcohol, HCl, NaOH, NaCl, H_2SO_4 were purchased from Sigma-Aldrich Chemical Reagents Co., Ltd. All other reagents were of analytical grade. Anionic dye Orange II (O II) and cationic dye methylene blue (MB), as the targeted adsorbates were employed during the batch adsorption experiments both in single and binary systems in this study. Molecular characteristics and structure of the two dyes are given in Fig. 1 and Table 1. All solutions were prepared using deionized water.

2.2. Synthesis of mesoporous carbon

The mesoporous carbon (MC) was synthesized using SBA-15 as template under acidic conditions and furfuryl alcohol as the carbon source through the following procedure [22]: In brief, 2.5 g of Pluronic P123 was dissolved in 12.59 mL of HCl (37 wt%) at 35°C under stirring with a magnetic stirrer. Then 5.85 mL of tetraethyl orthosilicate (TEOS, 98%, Sigma-Aldrich) was added to mixture solution under vigorous magnetic stirring to form the homogeneous solution at 35°C. Finally, the mixture solution was magnetically stirred for another 24 h at 40°C and then hydrothermally treated. Afterwards, the sample was aged under static conditions for 24 h at 40°C and subsequently for
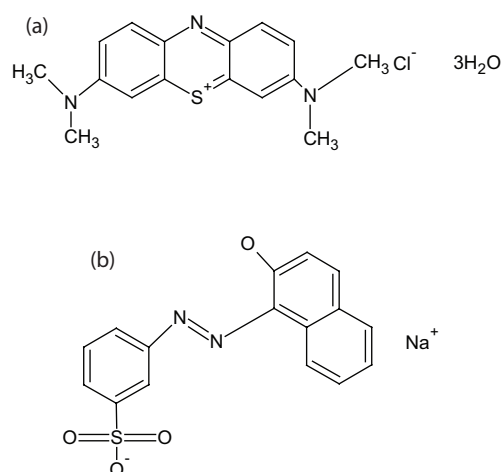

Fig. 1. Chemical structures of (a) MB and (b) O II.

Table 1
General characteristics of MB and O II

| Dye	Chemical class	Molecular weight (g/mol)	Molecular formula	λ_{max}(nm)
Methylene blue (MB)	Cationic dye	373.9	$C_{16}H_{18}CHN_3 \cdot 3H_2O$	665
Orange II (O II)	Anionic dye	350.3	$C_{16}H_{11}N_2NaO_4S$	485

another 24 h at 100°C. The obtained final product was filtrated with deionized water washing, dried at 60°C for 12 h, and then calcined in air by rising temperature from ambient at a rate of 5°C min⁻¹ to 550°C and maintain at that temperature for 12 h to remove the organic template. For the synthesis of mesoporous carbon samples according to the synthesis procedures as follows: first of all, 5 g of SBA-15 was impregnated with ethanol-aqueous solution ($V_{ethanol}$: $V_{aqueous\ solution}$ = 1:1) containing 5 g furfuryl alcohol and 0.5 mL oxalic acid for 24 h at 25°C. Afterwards, it was thermally heated at 105°C to polymerize for 24 h. Subsequently, the composite materials were carbonized at 900°C with a heating rate of 5°C min⁻¹ for 9 h in inert nitrogen atmosphere, the carbon product then was cooled to room temperature under a nitrogen atmosphere. Finally, the silica template was dissolved with 1.0 M NaOH ethanol solution (the volume ratio = 1:1) twice at 100°C for 1 h. And the resulting nanocomposites were filtered, washed with distilled water and ethanol, and dried at 105°C for 12 h. The samples were labeled as MC.

2.3. Amine-functionalization of mesoporous carbon

The functionalization of mesoporous carbon was carried out in the furnace system under high temperature. The as-prepared mesoporous carbons were placed in quartz tube furnace with quartz boat. The loading of nitrogen-doped functional groups onto the surface of mesoporous carbons were carried out by applying heat treatment with ammonia gas at the desired temperature. Typically, the sample materials were first heated to 300°C with the heating rate of 10°C min⁻¹ for 3 h in nitrogen gas condition to remove impurities. Afterwards, the furnace was heated to 900°C under the same conditions and subsequently the gas was switched to ammonia gas, and then the temperature was maintained at the same for 1 h (the flow rate of ammonia gas about 60 cm³ min⁻¹). Subsequently, the treatment tubular furnace system was converted to nitrogen and the samples were cooled to room temperature under nitrogen atmosphere. After cooling to room temperature, the resulting black solids were filtered and thoroughly washed several times with deionized water until a neutral pH of the residual liquid was reached, followed by drying at 105°C overnight. The samples were labeled as AFMMC.

2.4. Magnetization of mesoporous carbon

AFMMC composites were synthesized through co-precipitation method [23]. First, 0.25 mg of $FeCl_2 \cdot 4H_2O$ and 0.50 mg of $FeCl_3 \cdot 6H_2O$ were dropwise slowly dissolved in contains the fraction amount of mesoporous carbon water solution (10 mL), followed by strong continuous agitation. Afterward, 10 mL of $NH_3 \cdot H_2O$ was pumped in the mixture iron solution while stirring vigorously. The flask was connected to nitrogen gas and placed in a water bath was raised at heat rate of 5°C min⁻¹ to 70°C and maintained with constant stirring at this temperature about 4 h. Next, the resulting mixtures were slowly heated and continuously stirred for 2 h. Finally, the loaded products were collected by magnet, washed several times with distilled water until the pH close to 7 in the residual liquid, and then dried and stored in desiccator until it was used. The AFMMC were formed through the following reaction:

$$Fe^{2+} + 2Fe^{3+} + 8OH^- \rightarrow Fe_3O_4 + 4H_2O \qquad (1)$$
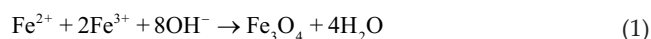
2.5. Structure characterization of as-prepared mesoporous carbons

The textural characterization of the mesoporous carbons composites were performed by N_2 adsorption/desorption isotherm at 77 K using a Quantachrome Autosorb 1. The specific surface area was calculated using the Bruamauer-Emmett-Teller (BET) equation. The element contents of carbon, hydrogen and nitrogen of MC and AFMMC were measured using elemental analyzer. The element contents of MC and AFMMC were measured using Physical Electronics PHI 5600 X-ray photoelectron spectroscopy (XPS) spectrophotometer apparatus with a monochromatic Al Kα radiation as excitation source. The surface functional groups of mesoporous carbons were analyzed using Fourier transform infrared (FT-IR) spectroscopy. The point of zero charge (pH_{PZC}) values of mesoporous carbon composites were determined by a mass titration method using pH meter. Magnetometer (AGM2900) was employed to analyze the magnetic properties of the samples at room temperature.

The pH_{PZC} of adsorbents were determined using pH a mass titration method by pH meter. Different amounts of the adsorbents were put in 50 mL 0.1 mol/L NaCl solutions (prepared in boiled water to eliminate CO_2). Then, the pH value of the mixture was adjusted to a value range between 2 and 12 using 0.1 M HCl or 0.1 M NaOH solutions. 0.1 g of carbon sample was added to each flask. The flasks were sealed and shaken in thermostat shaker overnight at 30°C, and the final equilibrium pH values of the suspensions solutions were analyzed. In addition, blank tests were also studied without adsorbent samples to eliminate other influences. Afterwards, the pH values of the blank test was measured and designated as $pH_{initial}$, the pH_{PZC} was taken as the point where the curve pH_{final} vs. $pH_{initial}$ crosses the line $pH_{initial} = pH_{final}$.

2.6. Batch adsorption experiments

Adsorption isotherms of O II or MB dye was determined both in single- and binary-component systems at different condition of parameters, using a thermostatic agitator. For the single-system adsorption experiments, 0.1 g of adsorbent was added to 50 mL conical tubes each containing 200 mg L⁻¹ of O II or MB solution. The effect of solution pH (2–12), initial concentration (range: 100–400 mg L⁻¹), salt concentration (range: 0–1 mol L⁻¹) and temperature (25°C–45°C) were investigated with the same amount of adsorbent. For the binary system adsorption experiments, the experiments were conducted by adding 0.1 g of adsorbents to 50 mL 200 mg L⁻¹ of initial concentrations that contained another component in a 100 mL flask. The solution pH was adjusted to the required value by adding a few drops of diluted 0.1 M HCl or 0.1 M NaOH solutions. Each experiment was duplicated under identical conditions.

2.6.1. Adsorption isotherms

For the single-system adsorption experiments, the batch experimental data were analyzed using Langmuir,

Freundlich, and Temkin adsorption isotherm models and their equations are given below [24,25]:

Langmuir model:

$$q_e = \frac{k_L C_e}{1 + k_L C_e} Q_m \qquad (2)$$

Freundlich model:

$$q_e = K_F C_e^{1/n} \qquad (3)$$

Temkin model:

$$q_e = B_1 \ln(A C_e) \qquad (4)$$

where q_e and C_e are the equilibrium adsorption capacity (mg g^{-1}) and the equilibrium concentration (mg L^{-1}); Q_m is the maximum amount of dye per unit weight of adsorbent for complete monolayer coverage (mg g^{-1}); K_L (L mg^{-1}), and K_F (mg g^{-1}) are Langmuir and Freundlich isotherm, respectively; n is a measure of the adsorption capacity and intensity. A (L g^{-1}) is the isotherm equilibrium constant, R (8.314 J mol^{-1} K^{-1}) is the gas constant, and T (K) is absolute temperature; b is the Temkin isotherm constant, related to the maximum binding energy, $B_1 = RT/b$.

For the binary system adsorption experiments, interaction of two components in binary mixtures could be evaluated by the ratio of adsorption capacity of one component in the binary solution (Q_{mix}) to the same component when present single (Q_{max}). The concentration of each component in the solution was measured using a UV/vis spectrometer at maximum wavelength, respectively. The multi-exponential model is an attractive candidate model for adsorption mechanisms studies that has multiple parallel routes that contribute to the total adsorbate amount. In this scenario, the adsorption equilibrium for binary-component systems, consisting of O II and MB dye were studied using competitive Langmuir, non-competitive Langmuir, and Langmuir–Freundlich isotherms [26–28].

Competitive Langmuir model:

$$q_{e,i} = \frac{Q_{max} K_{L,i} C_{e,i}}{1 + \sum_{j=1}^{N} K_{L,j} C_{e,j}} \qquad (5)$$

Non-competitive Langmuir model:

$$q_{e,i} = Q_{max} \left(\frac{K_{L,i} C_{e,i} + K_{L,jj} C_{e,i} C_{e,j}}{1 + K_{L,i} C_{e,i} + K_{L,j} C_{e,j} + K_{L,jj} C_{e,i} C_{e,j}} \right) \qquad (6)$$

Langmuir–Freundlich model:

$$q_{e,i} = \frac{K_{LF} C_{e,i}^{m}}{1 + K_{LF} C_{e,i}^{m}} Q_{max} \qquad (7)$$

where $q_{e,i}$ is the adsorbed concentration in equilibrium (mg g^{-1}), $C_{e,i}$ is the concentration of the liquid-phase adsorbate solution at equilibrium (mg L^{-1}), the coefficients i and j are the dyes present, Q_{max} is the maximum amount of dye concentration (mg g^{-1}), and K_L, K_{LF}, and m (dimensionless) are parameters of the isotherm model (K_L and K_{LF} are related to the energy of adsorption affinity).

2.6.2. Kinetic models

For the single-system adsorption process, batch sorption kinetic experiments were carried out in 500 mL flasks containing 300 mL of O II or MB dye solution (200 mg L^{-1}) with 0.1 g adsorbent, respectively. The flasks were agitated on a rotary shaker at 130 rpm under constant temperature (25°C). The samples were extracted at different time intervals, filtered and analyzed for the dye concentrations. The sorption kinetics of dye was investigated using the pseudo-first-order, pseudo-second-order, and intra-particle diffusion equation [29].

The pseudo-first-order equation is expressed as follows:

$$\ln(q_e - q_t) = \ln q_e - k_1 t \qquad (8)$$

where q_e and q_t are the amounts of O II or MB adsorbed (mg g^{-1}) at equilibrium and at time t (h), respectively; and k_1 (h^{-1}) is the rate constant adsorption of pseudo-first-order equation.

The pseudo-second-order equation can be expressed as:

$$\frac{t}{q_t} = \frac{1}{k_2 q_e^2} + \frac{t}{q_e} \qquad (9)$$

where q_e and q_t are the amounts of O II or MB adsorbed (mg g^{-1}) at equilibrium and at time t (h); k_2 (g mg^{-1} h) is the rate constant of the second-order equation.

The well-known form of intra-particle diffusion equation is given by:

$$q_t = k_p t^{1/2} + C \qquad (10)$$

where q_t are amounts of O II or MB adsorbed over a given period of time t; t is the adsorption time (min); k_p (mg g^{-1} h) are the adsorption rate constants of the intra-particle diffusion, and C (mg g^{-1}) is a constant in the intra-particle diffusion equation, corresponding to the thickness of boundary layer.

2.7. Regeneration test

The reusability and recycle experiment is useful to determine the adsorption mechanism and provide valuable information about the irreversibility of the adsorption process [30]. In this study, the regeneration and recycle procedures comprised of two steps. The regeneration of AFMMC adsorbent was carried out using ethanol, methanol and acetone solution at 25°C. The dye-loaded AFMMC were added with 50 mL of desorption reagent and shaken for 4 h, and the AFMMC in each flask were magnetically separated, washed and dried for

the next adsorption. To determine the reusability of AFMMC, the regenerated adsorbents were used for another adsorption, and the consecutive adsorption–regeneration cycle process was repeated for four times using the same adsorbent.

3. Results and discussion

3.1. Characterization of adsorbent

Fig. 2 shows the isotherms of N_2 adsorption/desorption and the pore size distribution of the mesoporous carbon materials. The curves in Fig. 2 show the presence of a hysteresis loop in the range of 0.4–0.6 P/P_0 onto the mesoporous carbon's surfaces, according to IUPAC classification, indicating that the adsorbents exhibit a type IV uniform mesoporous structure and contain a larger amount of mesopores in the material. The pores in the structures of these mesoporous carbon materials are mainly located in the mesoporous region [31].

The porosity had a strong effect on the adsorption properties of the mesoporous carbon materials. The mesoporous nanocomposites exhibited a high surface area, large pore volume, and narrow, uniform pore size distribution. The analysis revealed that the two adsorbents have a pore structure and the narrow pore size distribution of 2–4 nm, BET surface areas, and micropore and mesopores volumes of 1,185 and 1,290 m^2 g^{-1}, 3.4 and 3.6 nm, and 0.83 and 0.89 cm^3 g^{-1}, respectively (Table 2). The N_2 adsorption–desorption analysis indicates that the AFMMC materials have a higher specific surface area and pore volume, as the

introduction of the amine-functionalized process can provide more adsorption sites. The decrease in the micropore volume during the activation process could be because the activation reaction of mesoporous carbon became more severe under a high temperature, therefore, some micropores transformed into larger pores (mesopores), resulting in the formation of more mesopores in the raw MC [32]. Following this, the pore structure decreased to a certain extent, along with the loading of iron nanoparticles embedded into the pores of the nitrogen-doped graphitized mesoporous carbon matrix.

Amine-functionalization lead to an increase in the textural properties, which might be because the thermal decomposition of functional oxygen groups improved the specific surface area and pore volume, indicating the development of new pores and widening of existing pores during the ammonia-tailored activation process. Moreover, this decreasing trend in the textural properties was observed due to the pore filling effect of iron nanoparticles, and an excessive amount of nanoparticles was introduced to the mesoporous carbon's framework or attached to its surface.

The elemental analyses of the raw MC and AFMMC are presented in Table 3. When the functional amine groups were introduced to the surface of the mesoporous carbon, the process was found to change the total surface area and volume, as mentioned above; however, the surface morphology of the mesoporous carbon materials were almost the same. The elemental analyses of the raw MC and AFMMC changed after ammonia modification, and the results are shown in Table 3. The nitrogen carbon content increased significantly after the activation process, while the hydrogen, carbon, and oxygen contents decreased significantly. This could be due to the burn-off of carbon under the high temperature during prolonged activation. The nitrogen content of AFMMC increased after activation, indicating that nitrogen-containing surface functional groups were successfully introduced to the adsorbent's surface. In addition, iron was added through the magnetization process, indicating that the iron oxide nanoparticles have successfully dispersed into the matrix of the AFMMC.
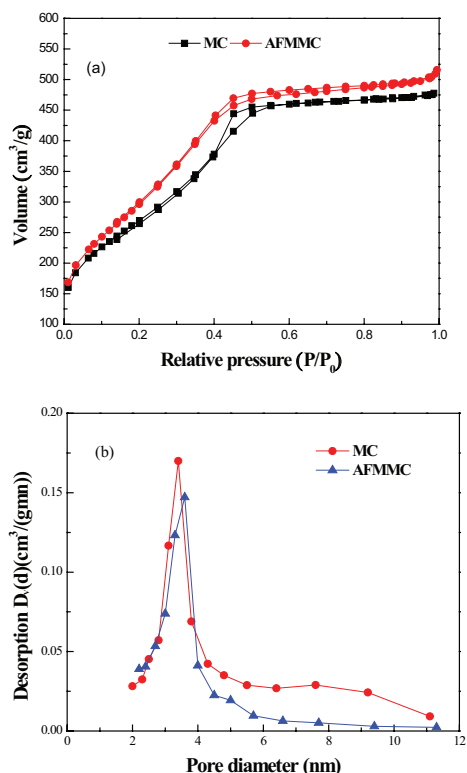

Fig. 2. N_2 adsorption/desorption isotherms of MC and AFMMC. (a) Nitrogen adsorption/desorption isotherms and (b) pore size distributions by BJH method.

Table 2
Pore textural characteristics of virgin MC and AFMMC

Samples	MC	AFMMC
S_{BET} (m^2 g^{-1})	1,185	1,290
V_T (m^3 g^{-1})	1.05	1.17
V_{mic}	0.221	0.124
D_P (nm)	3.4	3.6

Table 3
Elemental composition analysis of the raw MC and AFMMC

Sample	Raw MC	AFMMC
C (%)	91.32	84.71
N (%)	0.18	6.32
O (%)	8.22	2.18
H (%)	2.31	1.05
Fe (%)	0	2.15

Fourier-transform infrared spectroscopy (FTIR) was used to investigate the ammonification process, and results between 400 and 4,000 cm⁻¹ are presented in Fig. 3. The observed additional characteristic peaks of AFMMC indicated a high amount of nitrogen-containing bonds on the surfaces, which may have been the result of the ammonification modification process. In addition, the thermal treatment is responsible for eliminating or rearranging the functional groups on the adsorbent's surface. For instance, the presence of a new absorption band, that is, the peak at 3,135 cm⁻¹, is related to the –NH stretching vibration of the primary amide group. Furthermore, the peak at 1,660–1,400 cm⁻¹ could be attributed to the amino functional group, and can be attributed to N–H bending vibrations [33]. These results suggest that nitrogen-containing groups were grafted onto the surface of the MC by the modification process. Several peaks were changed, for example, the intensities of the peaks at 3,400 cm⁻¹ and 1,215–1,219 cm⁻¹ were reduced significantly, which could be attributed to the thermal treatment as it may have eliminated some functional groups on the adsorbent's surface. The peaks at 600–400 cm⁻¹ are assigned to the stretching of the Fe–O in Fe_2O_3 and Fe_3O_4 from bending vibration. It can be further concluded that the iron nanoparticles were successfully attached to the adsorbent's frame, which is consistent with the analysis of the EA results. This may be because the sorption behavior of the adsorbent was affected by the surface functional groups or it was mainly governed by chemical adsorption [34].

It was also found that ammonia gas treatment was a highly effective preparation method for doping N atoms into the carbon matrix under a high treatment temperature. To further understand the features of the surface nitrogen species, high-resolution XPS spectra of N 1s were obtained from the raw MC and AFMMC, as shown in Table 4. The XPS analysis confirmed that N and Fe species were successfully grafted to the MC surface, and the results indicated the presence of C, N, O, and Fe in the AFMMC. Ammonia gas can act as an important activation agent for mesoporous carbon. The AFMMC samples contained a high amount of N on their surfaces, which were provided by the high-temperature ammonification process, and their O content significantly decreased. This could be due to the number of N-group
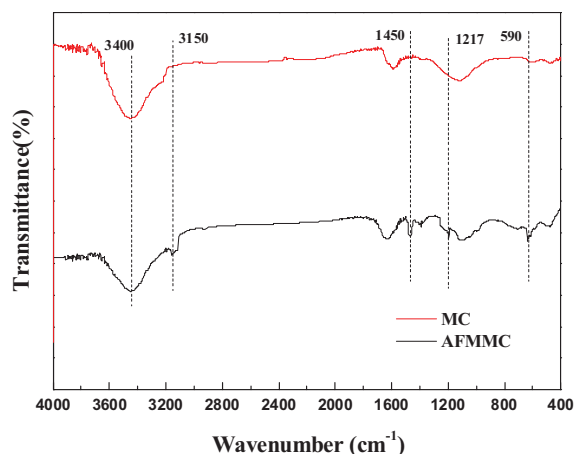
sites present on the carbon's surface, as many of the oxygen groups decomposed, leaving vacant sites. However, there was still a small amount of oxygen-containing species after treatment with gaseous ammonia at higher temperatures. These XPS results were consistent with the results of previous FTIR and EA analyses [35]. Further, the appearance of Fe2P indicated that some new species were incorporated into the adsorbent's surface.

XPS was a successful method for studying the nitrogen-containing functional groups on the material's surface. The high-resolution N1s XPS spectra peaks of the amine-functionalized mesoporous carbons are shown in Fig. 4. The N1s spectrum region indicates that the presence of the four primary types of N-containing composites formed on the sample's surface due to ammonization, and include pyridine-like nitrogen (398–399 eV), aromatic amines (400–400.5 eV), quaternary nitrogen (401–402 eV), and protonated amide (403–403.2 eV), which mainly consists of N-containing functional groups that would create a more hydrophobic surface and increase the composite's affinity to hydrophobic organic compounds. These results further confirm that the surface of the MC was amine-functionalized [36].

Fig. 5 shows that the pH_{PZC} values of MC and AFMMC were approximately 6.7 and 8.3, which indicates the basic characteristics of an adsorbent surface. This can be attributed to the significant amount of N species on the mesoporous carbons, and further indicates that functional amino groups were successfully grafted onto the surface, creating a surface that was positively charged and leading to an increase in the pH_{PZC} values.

Table 4
XPS of the raw MC and AFMMC

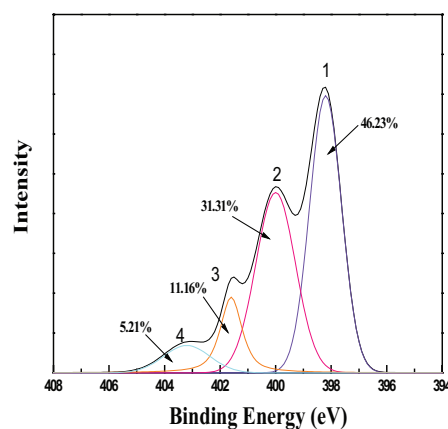| Sample	Raw MC	AFMMC
C1s (at%)	91.55	87.82
N1s (at%)	0.02	6.78
O1s (at%)	6.75	2.31
Fe2p (at%)	0	1.04

Fig. 3. FTIR spectra of the raw MC and AFMMC.

Fig. 4. High resolution N1s XPS spectra of the typical nitrogen functional groups on the AFMMC: (1) pyridine-like nitrogen, (2) aromatic amines, (3) quaternary nitrogen, and (4) protonated amide.
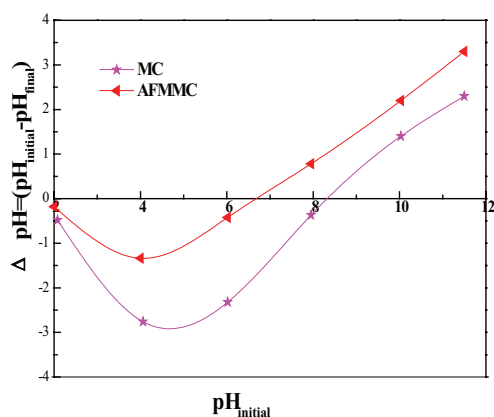
Fig. 5. pH$_{PZC}$ of raw MC and AFMMC.

Fig. 6. Magnetization curves measured for AFMMC.

The magnetic properties of the prepared AFMMC were measured at room temperature (25°C) under an external magnetic field ranging from –30,000 to 30,000 Oe, and the obtained magnetic curves are presented in Fig. 6. The presence of a magnetic hysteresis loop indicates that the AFMMC has superparamagnetic characteristics, with a saturation magnetization value (M) of approximately 4.53 emu g^{-1}, as shown in Fig. 6 (inset). The functionalized magnetic AFMMC nanoparticles could be easily separated and collected from the aqueous solution using an external magnet.

In conclusion, All the above analyses proved that amino functional groups and magnetic nanoparticles were successfully grafted onto the adsorbent surface and frame.

3.2. Adsorption of dye in single system

3.2.1. Effect of solution pH

The effect of solution pH on the dye adsorption capacities of the raw MC and AFMMC was studied at an initial dye concentration of 500 mg L^{-1}, dosage of 0.03 g/50 mL, and adsorption temperature of 25°C. Fig. 7 shows the effect of solution pH on the removal of O II or MB by the raw MC and AFMMC. For the cationic dye, MB, the removal efficiency quickly increased as the pH increased from 2 to 7, reached the maximum adsorption at approximately pH 7, and then slightly increased as the pH exceeded 7.0. The lower adsorption of MB dyes under low-pH conditions is due to the presence of excess hydrogen ions (H$^+$), which competed with dye cations for the limited adsorption sites of the adsorbent. At a higher solution pH, the mesoporous carbon's surface became negatively charged due to the deprotonation of the adsorbent's surface and the formation of an electrostatic double layer, which changes its polarity, therefore, the MB dye sorption increases [37]. Such trends can be explained by the increased uptake of MB onto the mesoporous carbons, which is due to the neutralization of the negative sites at the adsorbent's surface that facilitates diffusion and provides a larger active adsorption surface, resulting in enhanced uptake. As the pH of the solution gradually increased, the number of ionizable sites on mesoporous carbons also increased.

In addition, as shown in Fig. 5, the experimental pH$_{PZC}$ of MC and AFMMC were 6.7 and 8.3, respectively. The maximum amount of adsorbed MB dye solution concentrations (about
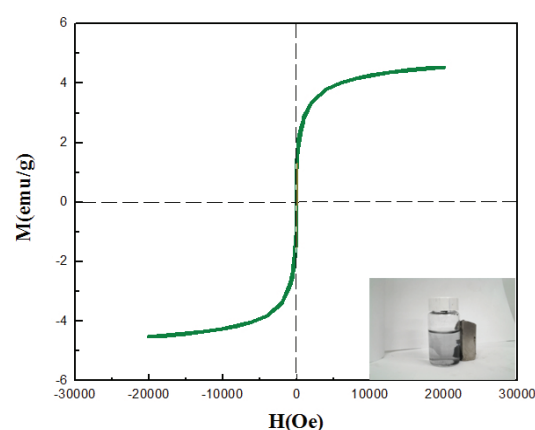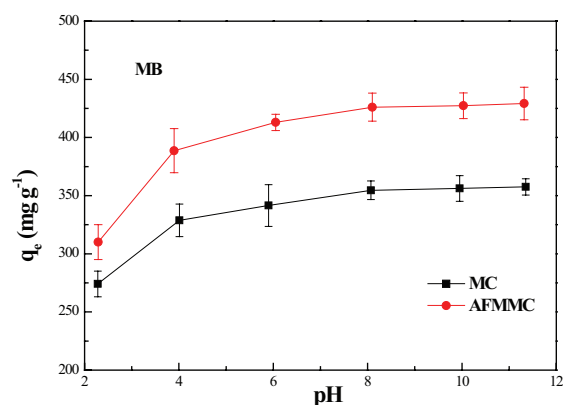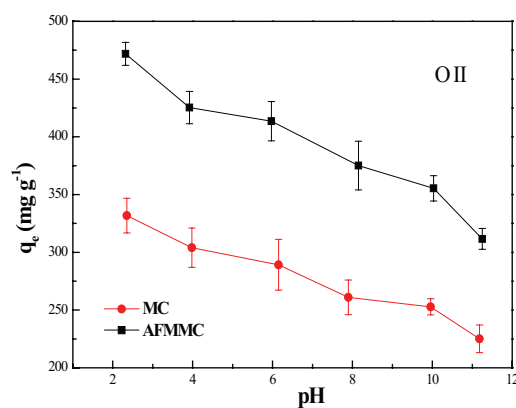

Fig. 7. Effects on the adsorption of O II or MB onto the raw MC and AFMMC at different initial pH.

pH = 8) is slightly above the zero point charge (pH$_{PZC}$ = 6.7), deducing that the surface negative charge density of mesoporous carbons increased which favors the adsorption of cationic dye. However, the opposite trend of anionic dye O II adsorption amount was also observed. It can be seen from the highest O II adsorption capacity at pH 2, the amount of O II anionic dye adsorbed on the mesoporous carbons tended to drastically decrease with an increase in solution pH from 2 to 12, which could be attributed to the electrostatic interactions. It was obviously observed that the maximum adsorption of

O II at pH 2 was due to the strong electrostatic attraction between the negatively charged deprotonated O II dye and positively charged mesoporous carbons surface. But with an increase in solution pH, the strong electrostatic repulsion increased between the negatively charged surface and O II anionic dye molecules, thus decreasing the adsorption capacity. This observation is similar to reports of Han et al. [38]. Taking into account these facts, it was concluded that the best pH to remove O II and MB dyes was at pH = 2 and pH = 8. Therefore, the next series of adsorption experiments were chosen at pH = 2 and pH = 8 as an optimum pH value for the next batch study.

3.2.2. Effect of salt concentration

Fig. 8 shows the effect of NaCl on the percentage removal of O II or MB. The presence of salt significantly influenced the adsorption rate of O II or MB, as the adsorption of O II or MB dye molecules to the adsorbent increased with the addition of NaCl. For AFMMC, the adsorption equilibrium of O II increased from 396.2 to 523.7 mg g^{-1} with the addition of NaCl, and that of MB increased from 345.8 to 475.6 mg g^{-1} as the NaCl concentrations increased from 0 to 0.1 mol L^{-1}, and then remained constant as the NaCl concentration continued to increase from 0.1 to 1 mol L^{-1}. This suggests that the salt concentration has an important influence on the adsorption of O II or MB dyes to the two mesoporous carbons. This is mainly due to the increase in ionic strength,

which can enhance the adsorption of ionic compounds, such as O II or MB dyes, due to the screening effect of the surface charge and the reduced electrostatic repulsion by the added salt. Therefore, an increase in the ionic strength will increase adsorption. However, this result does not agree with the results of the adsorption of methylene blue onto natural zeolite [39]. MC and AFMMC should be used to efficiently remove O II or MB from an aqueous solution with an appropriate amount of added salt.

3.2.3. Effect of temperature

Temperature is an important parameter in the dye adsorption process. The rate of dye molecule diffusion across the external boundary layer and in the internal pores of the adsorbent increased with increasing temperature, which changed the equilibrium capacity of the adsorbent [40].

As shown in Fig. 9, there was a high affinity between the surfaces of the two mesoporous carbons and dye molecules. For both the O II and MB dyes, the equilibrium adsorption amount increased as the temperature increased from 25°C to 45°C, indicating that the adsorption of the two dyes favored higher temperatures. This is likely because there was an increase in the number of new active sites on the raw MC and AFMMC for adsorption and with an increase in temperature as the adsorbent polarity and hydrogen bonding decreased, therefore, more sites were available for O II or MB
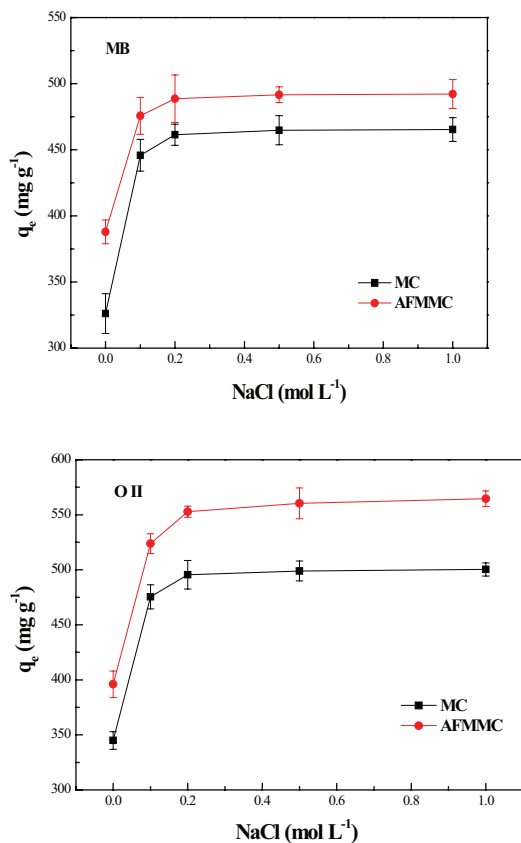

Fig. 8. Effects of NaCl concentration on the adsorption of O II or MB onto the raw MC and AFMMC.
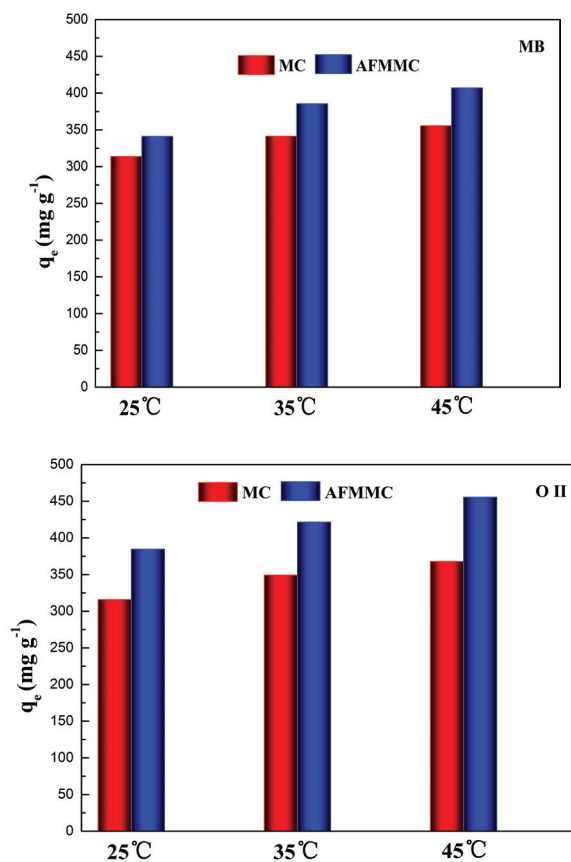

Fig. 9. Effects of temperature on the adsorption of O II or MB on the raw MC and AFMMC.

uptake. This may also be due to the increase in the mobility of the O II or MB molecules in the solution with the increase in temperature. This suggests that the removal of O II or MB by the mesoporous carbons involves a physical process in the overall adsorption mechanism. An increasing number of O II or MB dye molecules may acquire sufficient energy to interact with the active surface sites. The temperature dependence of the dye adsorption capacity suggests that the solubility of the O II or MB dye increases with increasing temperature as the amount of dye penetrating the inner pores of the mesoporous carbons increases. Additionally, this behavior indicates that the adsorption of the two dyes on the raw MC and AFMMC was endothermic in nature. A similar result was observed for the adsorption of methylene blue onto bamboo-based activated carbon [25].

3.2.4. Adsorption isotherms of single-component system

According to the results of the dye adsorption isotherm experiments, the adsorption capacity of O II onto the MC and AFMMC was higher than that of MB. Therefore, the raw MC and AFMMC have a stronger affinity for anionic O II dye than that for cationic MB dye. In this study, three adsorption isotherm models, that is, the Langmuir, Freundlich, and Temkin isotherms, were used to describe the results, and the results are presented in Table 5. The experimental adsorption data of the O II or MB dyes onto the raw MC and AFMMC were well described by the Langmuir isotherm model as it produced better correlation regression coefficients (R^2) for the adsorption of the two dyes than the other models at other temperatures, further demonstrating that the O II and MB dye molecules underwent monolayer adsorption onto the raw MC and AFMMC. The fitting isotherm of AFMMC from the Langmuir model exhibited maximum adsorption capacities of 389.6 and 325.3 mg g⁻¹ for the O II and MB dyes at 35°C, respectively.

In addition, the rapid uptake of anionic O II dye could be due to stronger affinity of amine groups for O II dye molecules than that for cationic MB dye molecules. The loading of ammonia on mesoporous carbons significantly affected anionic O II dye adsorption. The K_L value indicates the affinity for the binding of dye molecules; a high value indicates higher affinity. The values of Langmuir parameters Q_m and K_L increased as the temperature increased from 25°C to 45°C, indicating that the adsorption capacity and intensity were enhanced at higher temperatures. The values of K_F also increased with the increase in temperature, indicating that the adsorption process is endothermic. Additionally, a higher K_F value indicates that the raw MC and AFMMC possess a higher adsorption capacity for O II or MB dyes, and an n value below 1 indicates favorable adsorption of dyes by the raw MC and AFMMC [20]. Table 6 shows the maximum O II or MB dye adsorption capacities of some adsorbent materials reported in previous studies. The O II and MB adsorption capacities of AFMMC were relatively higher than those reported in some previous works.

3.2.5. Adsorption kinetics of single-component system

The adsorption rate is an important factor when selecting a material to be used as an adsorbent. To evaluate the kinetics

Table 5
Adsorption isotherm constants and correlation coefficients for the adsorption of O II and MB dye onto the MC and AFMMC at different temperature

Model	Constants	MC O II 25°C	MC O II 35°C	MC O II 45°C	MC MB 25°C	MC MB 35°C	MC MB 45°C	AFMMC O II 25°C	AFMMC O II 35°C	AFMMC O II 45°C	AFMMC MB 25°C	AFMMC MB 35°C	AFMMC MB 45°C
Langmuir	Q_m (mg g⁻¹)	183.4	236.5	264.7	174.4	212.5	241.7	312.5	389.6	415.6	284.5	325.3	354.3
	K_L (L mg⁻¹)	0.034	0.124	0.231	0.043	0.321	0.578	0.121	0.446	0.875	0.089	0.235	0.343
	R^2	0.996	0.999	0.997	0.999	0.998	0.999	0.995	0.998	0.999	0.998	0.997	0.998
Freundlich	K_F (mg g⁻¹)	78.99	132.5	223.5	85.65	125.7	185.4	188.6	277.6	307.4	152.3	191.1	223.1
	n	0.023	0.046	0.793	0.321	0.156	0.218	0.126	0.412	0.112	0.034	0.057	0.078
	R^2	0.898	0.948	0.976	0.889	0.974	0.899	0.875	0.919	0.921	0.933	0.889	0.936
Temkin	B	98.76	196.65	213.56	112.34	156.65	213.65	137.32	213.43	278.32	115.32	194.43	224.56
	A (L mg⁻¹)	0.032	0.441	0.654	0.234	0.467	0.765	0.231	0.551	0.644	0.325	0.658	0.823
	R^2	0.931	0.965	0.977	0.972	0.986	0.991	0.933	0.968	0.983	0.988	0.899	0.956

of the sorption of O II or MB onto the raw MC and AFMMC, kinetic data were investigated by pseudo-first-order, pseudo-second-order, and intraparticle diffusion models.

As shown in Table 7, the calculated q_e values are not consistent with the experimental values; therefore, the pseudo-first-order model did not fit the data well. However, the R^2 values of the pseudo-second-order model were higher than those of the pseudo-first-order and intra-particle diffusion models, and the calculated $q_{e,cal}$ values were closer to the experimental values than those of the other two models. Therefore, the pseudo-second-order kinetic model could describe the adsorption kinetics data more favorably. This suggests that the pseudo-second-order adsorption mechanism is predominant, and that the overall rate of dye adsorption appears to be controlled by the chemisorption adsorption process. The plot of q_t against $t^{1/2}$ should be linear and pass through the origin, so the intra-particle diffusion model was used to determine the rate-limiting step of the adsorption process. It could be concluded that both surface adsorption and intra-particle diffusion occurred simultaneously during the adsorption process [47,48].

3.2.6. Thermodynamic studies of single-component system

An increase in the temperature resulted in an increase in the adsorption capacity for the two dyes (Fig. 10). To better estimate the effect of temperature on the adsorption of O II and MB onto the mesoporous carbons, thermodynamic parameters, including the enthalpy (ΔH), entropy (ΔS),

and Gibbs free energy (ΔG), were determined using the following equations [49]:

$$\Delta G = -RT \ln k_L \tag{11}$$

$$\ln k_L = \frac{\Delta S}{R} - \frac{\Delta H}{RT} \tag{12}$$

where ΔG is the change in the Gibbs free energy (kJ mol^{-1}), and ΔS (J (K·mol)$^{-1}$) and ΔH (kJ mol^{-1}) are the changes in the entropy and enthalpy of adsorption. K_L represents the Langmuir constant, R is the gas universal constant (8.314 J mol K^{-1}), and T is the absolute temperature.

The calculated ΔH, ΔS, and ΔG values are listed in Table 8. The positive ΔH value (O II or MB) at the three temperatures

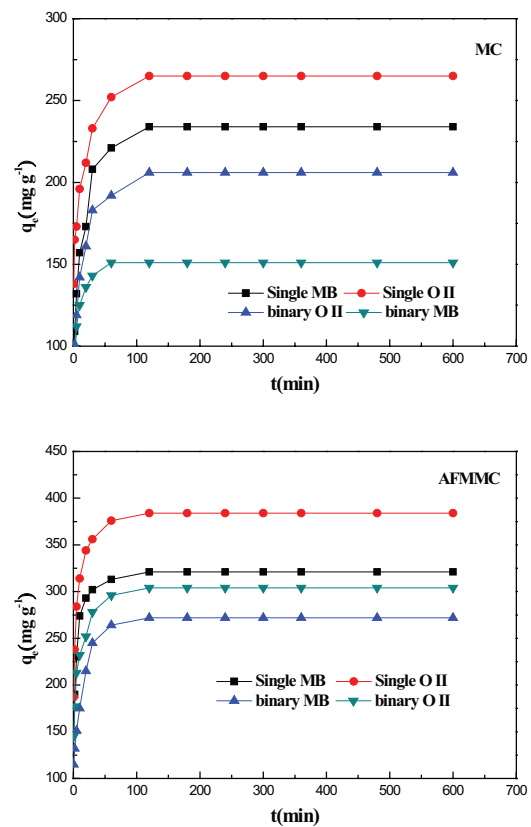Fig. 10. Adsorption isotherms of O II or MB in the presence and non-presence of another dye on the MC and AFMMC.

Table 6
Comparison of the maximum adsorption capacity of different adsorbents for dyes

Material	Maximum adsorption capacity (mg g^{-1})	Reference
Activated biochar	161.3 (MB dye)	[41]
Chitosan/activated charcoal	250.0 (MB dye)	[42]
Montmorillonite/CoFe$_2$O$_4$	97.75 (MB dye)	[43]
Montmorillonite	118.62 (O II dye)	[44]
Activated carbon	310.89 (O II dye)	[45]
Surfactant-coated zeolite	38.96 (O II dye)	[46]
AFMMC	389.6 (O II dye)	This work
AFMMC	325.3 (MB dye)	This work

Table 7
Fitted parameters summary of kinetics of O II or MB dyes sorption onto the raw MC and AFMMC

Dye	Adsorbent	q_{exp}	Pseudo-first-order			Pseudo-second-order			Intraparticle diffusion		
			$k_1 \times 10^{-2}$	q_e	R^2	$k_2 \times 10^{-3}$	q_e	R^2	k_p	C	R^2
O II	Raw MC	275.8	4.32	89.6	0.953	0.77	255.4	0.997	12.33	45.76	0.986
	AFMMC	382.5	5.75	189.8	0.944	0.91	367.3	0.999	43.54	32.52	0.988
MB	Raw MC	263.2	3.84	101.2	0.962	0.68	233.1	0.996	27.52	55.88	0.979
	AFMMC	311.8	4.59	142.3	0.977	0.71	285.6	0.998	69.23	41.44	0.978

Table 8
Thermodynamic parameters of the adsorption of O II or MB dye onto the raw MC and AFMMC under different temperature

Dye	Adsorbent	ΔH (kJ mol^{-1})	ΔS (kJ mol^{-1} K)	ΔG (kJ mol^{-1})		
				25°C	35°C	45°C
O II	Raw MC	25.3	0.22	–18.3	–21.6	–23.5
	AFMMC	37.6	0.48	–27.1	–29.3	–31.8
MB	Raw MC	21.4	0.17	–17.5	–20.4	–22.7
	AFMMC	33.5	0.35	–22.3	–25.6	–28.4

(25°C, 35°C, and 45°C) reveals that the adsorption process is favorable and endothermic in nature. The diffusion rate of O II or MB dye molecules increased as the temperature increased. Therefore, large amounts of O II or MB dye will be adsorbed as a large number of active sites were utilized across the external boundary layer and the internal pores of the mesoporous carbons. The negative value of ΔS indicates that the order of reaction is higher during the adsorption of O II or MB dye onto the mesoporous carbons, which could be due to a combination of the affinity of mesoporous carbons for O II or MB dye at the solid–solution interface. The negative value of ΔG confirms that the adsorption of O II or MB dye onto the raw MC and AFMMC is feasible, and that the adsorption process is spontaneous in nature. The negative ΔG value confirms that adsorption was more favorable as the temperature increased, suggesting that the adsorption spontaneity and the force driving the adsorption of both O II and MB are proportional to the temperature, which is consistent with the experimental result. Additionally, the adsorption process is endothermic in nature. This behavior can be interpreted considering the electrostatic repulsion between the adsorbent and adsorbate, as the process draws some energy from the environment to overcome the repulsion force and move the ionic dye closer to the adsorbent. Therefore, a higher adsorption capacity was achieved at a higher temperature [50].

3.3. Adsorption of dye in binary-component system

As wastewater often contains a mixture of dyes, their coexistence may affect their adsorption efficiencies, therefore, an efficient adsorbent with a high adsorption capacity must be used to remove the mixture of dyes from wastewater. To evaluate the effect of the coexistence of dye molecules on their adsorption onto the adsorbents, the sorption of O II or MB dye in the presence of another dye was investigated, and the results are shown in Fig. 10. It shows a comparison between the single- and binary-compound experimental data for both O II and MB dyes, and shows that the amount of O II or MB dye removed from the binary solution is less than that removed from the corresponding individual-component solution. This could be due to the occurrence of competition for the same adsorption sites on the adsorbent's surface [51].

When AFMMC was used to treat both dyes, the maximum amount of MB dye adsorbed decreased from 321 (in a single solution) to 275 mg g^{-1} (in the binary solution of O II and MB), and the maximum removal efficiency of O II dye decreased from 384 (in a single solution) to 302 mg g^{-1} (in a binary solution of O II and MB). These results suggest that

the presence of the other dye may change the main interactions responsible for adsorption and may, therefore, affect the adsorption mechanism. The O II or MB adsorption capacity of AFMMC was lower in the binary system than that of the single systems, which could be attributed to the competition between the two dyes for the active adsorption sites, resulting in a decrease in the adsorption capacity under the binary system adsorption. Additionally, this phenomenon could be due to the occupation of AFMMC adsorption sites by O II or MB molecules, as the steric hindrance of adsorbed molecules causes less dye to be removed from the binary solution. As shown in Fig. 10, the amounts of O II or MB adsorption to the MC exhibited a similar trend to those of AFMMC.

The adsorption efficiency of AFMMC was higher for O II dye than that for MB dye in the binary systems. This could be because O II is an anionic dye, therefore, it more readily adsorbs to the basic AFMMC surfaces due to the strong electrostatic interactions between the functional groups of the O II molecule and the AFMMC's surface. The presence of O II or MB has a negative effect on the sorption of the target pollutant, which might be due to interference and competition between the dyes for the specific sites on the adsorbent. However, the interference of the MB dye with the sorption of the O II dye was less intense. In a binary-component system, the affinity of both the adsorbate and adsorbent will change due to the competition for available adsorption sites. This might indicate that the adsorption of one adsorbate dye would mutually hinder and exclude the other dye. The affinity of O II for AFMMC was high, therefore, it was preferentially adsorbed onto the AFMMC over MB dye in binary systems. This is because the O II dye exhibited a stronger binding ability onto the AFMMC than the MB dye [52].

The conditions of binary systems are more complex; therefore, the effect of adsorption is complicated. To attain further insight into competitive adsorption in the binary system, the three equilibrium isotherm parameters of the adsorption of O II and MB dye onto the MC and AFMMC are listed in Table 9. This indicates that the isotherms of O II or MB dye in binary systems followed competitive and non-competitive Langmuir models, and the Langmuir–Freundlich model. The adsorption data for the two dyes verify that the Langmuir–Freundlich isotherm model represented the adsorption process more suitably than the competitive and non-competitive Langmuir models. The maximum amount of adsorbed O II dye derived from the three isotherms was larger than that of MB dye in binary systems. The negative value of this may indicate that O II and MB dye molecules could not simultaneously bond to the same binding site. Therefore, one binding site was only available for one dye molecule, and competitive

Table 9
Adsorption isotherms constants and correlation coefficients for the adsorption of O II and MB dye onto the MC and AFMMC in binary component system

Adsorbents	Dye	Competitive Langmuir			Non-competitive Langmuir					Langmuir–Freundlich			
		Q_{max}	$K_{L,i}$	R	Q_{max}	$K_{L,i}$	$K_{L,j}$	$K_{L,ji}$	R	Q_{max}	K_{LF}	M	R
MC	O II	142.4	1.54	0.867	133.4	7.84	9.51	3.54	0.932	209.3	15.4	0.13	0.996
	MB	121.2	1.39	0.897	162.3	4.31	2.37	5.32	0.897	184.5	11.7	0.23	0.994
AFMMC	O II	213.5	2.32	0.991	215.4	13.76	12.65	8.67	0.978	283.8	8.94	0.65	0.991
	MB	165.7	1.98	0.933	193.7	11.43	10.32	7.77	0.935	243.7	6.43	0.48	0.989

adsorption between O II and MB dye molecules occurred in the binary system [53]. In addition, as shown in Table 7, the values of $K_{L,i}$ and $K_{L,j}$ were higher for O II dye than those for the MB dye, further indicating the greater affinity between the O II dye and the adsorbents [28]. The above studies show that the O II dye was more easily adsorbed by AFMMC in the binary system of the two compounds. These results further indicate that the adsorption of OII dye on the AFMMC in both single and binary-component systems was higher than that of the MB dye.

3.4. Recycle and regeneration of AFMMC for dye removal from single and binary systems

The recyclability and regeneration efficiency is also an important factor for determining ideal adsorbents, therefore, the adsorption–desorption processes of the AFMMC were repeated four successive times in the single and binary systems, the AFMMC was collected using a magnet, and acetone and methanol were selected to test which was the most efficient solvent for regenerating MB and O II from the spent AFMMCs. After desorption, the regenerated AFMMC was magnetically separated and reused. The MB and O II adsorption capacity after four adsorption–desorption processes were tested, and the data are shown in Fig. 11.

For both the single and binary systems, the AFMMC exhibits excellent adsorption ability and efficiency for the MB and O II dyes using acetone and methanol as the eluent. During desorption, the decreasing trend of the MB or O II dye removal efficiency may be because some of the active sites of AFMMC were destroyed or blocked, resulting in a decreased MB and O II dye removal ability. However, there was no notable decrease in the adsorption capacity, and the ratio of adsorption loss did not exceed 20% in both the single and binary systems after undergoing the four repeated cycles. Therefore, there was no significant reduction in the active receptor sites on the AFMMC's surface. This indicates that the prepared adsorbent could efficiently prevent the discharge of secondary pollutants into the environment, and it exhibits excellent chemical stability and regenerative ability. Ai et al. [42] found that the introduction of iron ions will allow the spent adsorbents to be easily collected using a magnet, resulting in good recyclability, stability, and regenerative ability in the adsorption of dyes. In addition, the higher MB and O II adsorption efficiencies from the single-component solutions than those in the binary-component systems after
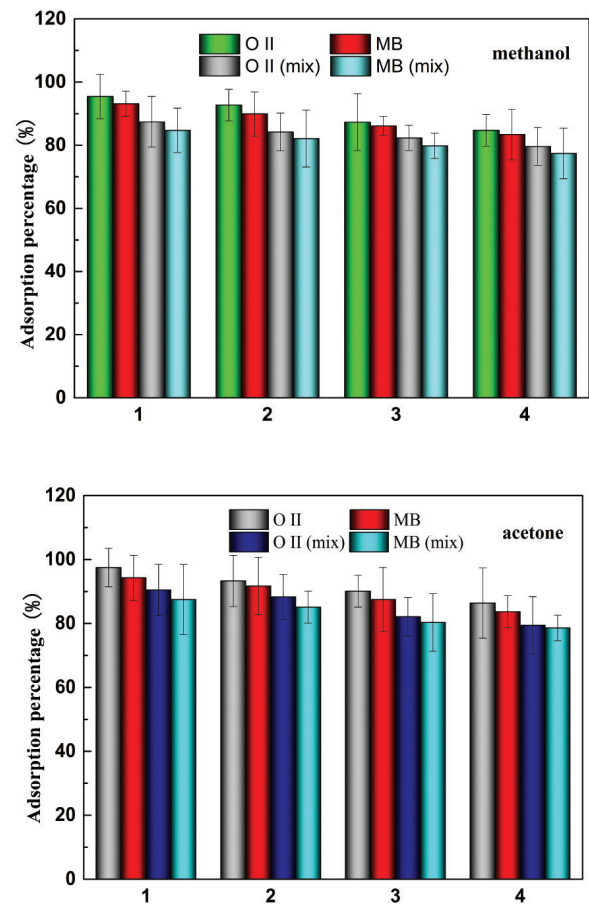

Fig. 11. Recycling performance of the AFMMC in removal of MB or O II dye from single and binary systems.

reuse confirm that competitive adsorption for the same adsorption sites occurred in the binary-component systems.

3.5. Adsorption mechanisms of process

All the above data proved that the MC and AFMMC exhibited excellent adsorption capacities toward MB and O II dye. Generally speaking, the molecular characteristics of dyes and the physico-chemical properties of an adsorbent play decisive role in adsorption process [54]. From the physical structure characterization, this remarkable improvement of AFMMC is explained by high surface area and pore

volume that are the most important parameters contributes to the sorption capacity, thus there exist enough hydrophobic sites by hydrophobic interactions and the pore-filling effect. Additionally, the pore-size distribution is one of the key factors governing the extent of dyes removal because dyes exhibit variable affinities for different surface functional groups and pore sizes. Modification of the MC materials remarkable improve its properties, as the AFMMC has more amino functional groups and availability of the adsorptive active sites compared with the raw MC, it is reasonable to make it possible for the adsorbent sufficiently to interact with dye molecules.

Other several important mechanisms might be involved in the adsorption processes by the interactions of both dyes and functional groups of adsorbents, including electrostatic attraction, hydrogen bond, planar aromatic structures, π–π interactions and hydrophobic interaction as driving forces affect the adsorption capacity [55]. From the front study of pH and zeta potential effect on adsorption efficiency, we could conclude that the electrostatic interaction plays an important role in the adsorption of two dye molecules onto the MC and AFMMC. Both acidic and basic groups were present on the surface of two adsorbents. However, The AFMMC had more basic groups than that of acidic groups and show positively charged character at higher pH values in comparison with origin, favoring uptake of more anionic groups due to increased electrostatic attraction between O II and the AFMMC surface. In the meantime, there are several nitrogen-containing functional groups, such as the –NH2, C–N groups may offer additional affinity and more available binding sites, and of which could via the formation of hydrogen bond with dye molecules facilitate dye diffusion and adsorption process. Furthermore, it is worth mentioning that the π–π electron donor–acceptor interactions and hydrophobic interactions between organic contaminants and graphitic sites on the two adsorbents are crucial for the organic contaminants removal process [56]. The hydrophobic interaction is another important factor effect on adsorption efficiency. Since the adsorbability of organic substances onto the adsorbents, the abundant amino functionalities provide the AFMMC composites with a strongly hydrophilic character, which easily facilitates the formation of more hydrophobic sites that contributed to its excellent adsorption performance of dye molecules. Besides, the influence of the iron oxide particles may play a major role in the adsorption of dye molecules; this phenomenon can be attributed to enhance the mobility of dye molecules in aqueous solution due to reduction of surface tension and viscosity of solutions, which is in favor for adsorption of dyes molecules onto the adsorbent surfaces [57].

3.6. Future research prospects

AFMMC were synthesized and investigated for the adsorption of anionic dye and cationic dye. The results displayed that AFMMC were deemed to be the promising adsorbent, with high removal for the two dyes from aqueous solutions, and the stability and recyclability was remarkable. The disadvantage of the material is that the preparation process is complicated and the preparation cost is relatively high. Therefore, the next step plan is to reduce the cost of preparation and carry out pilot test.

4. Conclusions

Herein, we report a feasible synthesis method for preparing recyclable and regenerable magnetic AFMMC as adsorbent for O II or MB dye in single and binary systems. FTIR, BET, XPS and Zeta potential measurements have been determined for characterizing the as-prepared nanocomposite. The nanomaterial exhibited the higher adsorption capacities and magnetic properties because of the introduction of nitrogen-containing functional groups and the impregnation of magnetic iron nanoparticles. The maximum adsorption capacities (Q_0) of AFMMC for O II and MB dyes were 389.6 and 325.3 mg g^{-1}, respectively. Moreover, the magnetic AFMMC could be easily separated from solution by an external magnetic field which will lead to a broad application prospects and its adsorption capacity could also be enhanced due to introduction of amino functional groups. The adsorption capacity of magnetic AFMMC still can reach about 80% to be reused four times using three eluent, indicating that AFMMC has high potential to be used repeatedly for dye removal. Furthermore, the results showed that the AFMMC is an adsorbent with a very high adsorption capacity capable of removing the anionic and cationic organic dyes from both single and binary systems.

References

[1] V. Nair, R. Vinu, Peroxide-assisted microwave activation of pyrolysis char for adsorption of dyes from wastewater, Bioresour. Technol., 216 (2016) 511–519.

[2] J. Fu, Q. Xin, X. Wu, Z. Chen, Y. Yan, S. Liu, M. Wang, Q. Xu, Selective adsorption and separation of organic dyes from aqueous solution on polydopamine microspheres, J. Colloid Interface Sci., 461 (2016) 292–304.

[3] S.P.D. Monte Blanco, F.B. Scheufele, A.N. Módenes, F.R. Espinoza-Quiñones, P. Marin, A.D. Kroumov, C.E. Borba, Kinetic, equilibrium and thermodynamic phenomenological modeling of reactive dye adsorption onto polymeric adsorbent, Chem. Eng. J., 307 (2017) 466–475.

[4] S. Liu, X. Feng, F. Gu, X. Li, Y. Wang, Sequential reduction/oxidation of azo dyes in a three-dimensional biofilm electrode reactor, Chemosphere, 186 (2017) 287–294.

[5] Y. Zheng, D. Chen, N. Li, Q. Xu, H. Li, J. He, J. Lu, Highly efficient simultaneous adsorption and biodegradation of a highly-concentrated anionic dye by a high-surface-area carbon-based biocomposite, Chemosphere, 179 (2017) 139–147.

[6] C.L. Zhang, J.J. Li, S.Y. Li, Photocatalytic degradation of pefloxacin in water by modified nano-zinc oxide, Mater. Lett., 206 (2017) 146–149.

[7] F. Liu, Z. Guo, H. Ling, Z. Huang, D. Tang, Effect of pore structure on the adsorption of aqueous dyes to ordered mesoporous carbons, Microporous Mesoporous Mater., 227 (2016) 104–111.

[8] X. Peng, F. Hu, T. Zhang, F. Qiu, H. Dai, Amine-functionalized magnetic bamboo-based activated carbon adsorptive removal of ciprofloxacin and norfloxacin: a batch and fixed-bed column study, Bioresour. Technol., 249 (2018) 924–934.

[9] X. Yue, T. Zhang, D. Yang, F. Qiu, Z. Li, Hybrid aerogels derived from banana peel and waste paper for efficient oil absorption and emulsion separation, J. Clean. Prod., 199 (2018) 411–419.

[10] V.K. Gupta, A. Nayak, S. Agarwal, I. Tyagi, Potential of activated carbon from waste rubber tire for the adsorption of phenolics: effect of pre-treatment conditions, J. Colloid Interface Sci., 417 (2014) 420–430.

[11] M. Kousha, E. Daneshvar, H. Dopeikar, D. Taghavi, A. Bhatnagar, Box–Behnken design optimization of Acid Black 1 dye biosorption by different brown macroalgae, Chem. Eng. J., 179 (2012) 158–168.

[12] I.A. Aguayo-Villarreal, V. Hernández-Montoya, E.M. Ramírez-López, A. Bonilla-Petriciolet, M.A. Montes-Morán, Effect of surface chemistry of carbons from pine sawdust for the adsorption of acid, basic and reactive dyes and their bioregeneration using *Pseudomonas putida*, Ecol. Eng., 95 (2016) 112–118.

[13] A. Pal, H.S. Kil, S. Mitra, K. Thu, B.B. Saha, S.H. Yoon, J. Miyawaki, T. Miyazaki, S. Koyama, Ethanol adsorption uptake and kinetics onto waste palm trunk and mangrove based activated carbons, Appl. Therm. Eng., 122 (2017) 389–397.

[14] K. Björklund, L.Y. Li, Adsorption of organic stormwater pollutants onto activated carbon from sewage sludge, J. Environ. Manage., 197 (2017) 490–497.

[15] J. Goscianska, N.A. Fathy, R.M.M. Aboelenin, Adsorption of solophenyl red 3BL polyazo dye onto amine-functionalized mesoporous carbons, J. Colloid Interface Sci., 505 (2017) 593–604.

[16] J. Galán, A. Rodríguez, J.M. Gómez, S.J. Allen, G.M. Walker, Reactive dye adsorption onto a novel mesoporous carbon, Chem. Eng. J., 219 (2013) 62–68.

[17] G. Zhou, B. Wu, X. Liu, Z. Li, S. Zhang, A. Zhou, X. Yang, Resistance switching characteristics of core–shell γ-Fe$_2$O$_3$/Ni$_2$O$_3$ nanoparticles in HfSiO matrix, J. Alloys Comp., 678 (2016) 31–35.

[18] Y. Wang, M. Yao, Y. Chen, Y. Zuo, X. Zhang, L. Cui, General synthesis of magnetic mesoporous FeNi/graphitic carbon nanocomposites and their application for dye adsorption, J. Alloys Comp., 27 (2015) 7–12.

[19] L.A. Kafshgari, M. Ghorbani, A. Azizi, Fabrication and investigation of MnFe$_2$O$_4$/MWCNTs nanocomposite by hydrothermal technique and adsorption of cationic and anionic dyes, Appl. Surf. Sci., 419 (2017) 70–83.

[20] T. Yao, S. Guo, C. Zeng, C. Wang, L. Zhang, Investigation on efficient adsorption of cationic dyes on porous magnetic polyacrylamide microspheres, J. Hazard. Mater., 292 (2015) 90–97.

[21] X. Peng, F. Hu, J. Huang, Y. Wang, H. Dai, Z. Liu, Preparation of a graphitic ordered mesoporous carbon and its application in sorption of ciprofloxacin: kinetics, isotherm, adsorption mechanisms studies, Microporous Mesoporous Mater., 228 (2016) 196–206.

[22] S.S. Samandari, H.J. Yekta, M. Mohseni, Adsorption of anionic and cationic dyes from aqueous solution using gelatin-based magnetic nanocomposite beads comprising carboxylic acid functionalized carbon nanotube, Chem. Eng. J., 308 (2017) 1133–1144.

[23] A. Regti, H.B.E. Ayouchia, M.R. Laamari, S.E. Stiriba, H. Anane, M.E. Haddad, Experimental and theoretical study using DFT method for the competitive adsorption of two cationic dyes from wastewaters, Appl. Surf. Sci., 390 (2016) 311–319.

[24] X. Peng, F. Hu, H. Dai, Q. Xiong, C. Xu, Study of the adsorption mechanisms of ciprofloxacin antibiotics onto graphitic ordered mesoporous carbons, J. Taiwan Inst. Chem. Eng., 65 (2016) 472–481.

[25] M. Arias, C. Pérez-Novo, E. López, B. Soto, Competitive adsorption and desorption of copper and zinc in acid soils, Geoderma, 133 (2006) 151–159.

[26] E.D. Freitas, A.C.R. Carmo, A.F.A. Neto, M.G.A. Vieira, Binary adsorption of silver and copper on Verde-lodo bentonite: kinetic and equilibrium study, Appl. Clay Sci., 137 (2017) 69–76.

[27] L. Li, F. Liu, X. Jing, P. Ling, A. Li, Displacement mechanism of binary competitive adsorption for aqueous divalent metal ions onto a novel IDA-chelating resin: isotherm and kinetic modeling, Water Res., 45 (2011) 1177–1188.

[28] F. Yu, S. Sun, S. Han, J. Zheng, J. Ma, Adsorption removal of ciprofloxacin by multi-walled carbon nanotubes with different oxygen contents from aqueous solutions, Chem. Eng. J., 285 (2016) 588–595.

[29] F. Jiang, D.M. Dinh, Y.L. Hsieh, Adsorption and desorption of cationic malachite green dye on cellulose nanofibril aerogels, Carbohydr. Polym., 173 (2017) 286–294.

[30] X. Peng, X. Hu, D. Fu, F.L.Y. Lam, Adsorption removal of acid black 1 from aqueous solution using ordered mesoporous carbon, Appl. Surf. Sci., 294 (2014) 71–80.

[31] X.G. Zhao, J.G. Huang, B. Wang, Q. Bi, L.L. Dong, X.J. Liu, Preparation of titanium peroxide and its selective adsorption property on cationic dyes, Appl. Surf. Sci., 292 (2014) 576–582.

[32] M.A.O. Lourenço, M.J.G. Ferreira, M. Sardo, L. Mafra, J.R.B. Gomes, P. Ferreira, Microwave-assisted N,N-dialkylation of amine-functionalized periodic mesoporous phenylene-silica: an easy and fast way to design materials, Microporous Mesoporous Mater., 249 (2017) 10–15.

[33] J. Gao, Y. He, X. Zhao, X. Ran, Y. Wu, Y. Su, J. Dai, Single step synthesis of amine-functionalized mesoporous magnetite nanoparticles and their application for copper ions removal from aqueous solution, J. Colloid Interface Sci., 481 (2016) 220–228.

[34] K. Liu, L. Chen, L. Huang, Y. Lai, Evaluation of ethylenediamine-modified nanofibrillated cellulose/chitosan composites on adsorption of cationic and anionic dyes from aqueous solution, Carbohydr. Polym., 151 (2016) 1115–1119.

[35] W. Song, B. Gao, T. Zhang, X. Xu, X. Huang, H. Yu, Q. Yue, High-capacity adsorption of dissolved hexavalent chromium using amine-functionalized magnetic corn stalk composites, Bioresour. Technol., 190 (2015) 550–557.

[36] D. Bharali, R.C. Deka, Preferential adsorption of various anionic and cationic dyes from aqueous solution over ternary CuMgAl layered double hydroxide, Colloid Surf., A, 525 (2017) 64–76.

[37] A. Rodríguez, J. García, G. Ovejero, M. Mestanza, Adsorption of anionic and cationic dyes on activated carbon from aqueous solutions: equilibrium and kinetics, J. Hazard. Mater., 172 (2009) 1311–1320.

[38] R. Han, J. Zhang, P. Han, Y. Wang, Z. Zhao, M. Tang, Study of equilibrium, kinetic and thermodynamic parameters about methylene blue adsorption onto natural zeolite, Chem. Eng. J., 145 (2009) 496–504.

[39] J. Cheng, L. Shi, J. Lu, Amino ionic liquids-modified magnetic core/shell nanocomposite as an efficient adsorbent for dye removal, J. Ind. Eng. Chem., 336 (2016) 206–214.

[40] M.A. Franciski, E.C. Peres, M. Godinho, D. Perondi, E.L. Foletto, G.C. Collazzo, G.L. Dotto, Development of CO$_2$ activated biochar from solid wastes of a beer industry and its application for methylene blue adsorption, Waste Manage., 78 (2018) 630–638.

[41] H. Karaer, İ. Kaya, Synthesis, characterization of magnetic chitosan/active charcoal composite and using at the adsorption of methylene blue and reactive blue4, Microporous Mesoporous Mater., 232 (2016) 26–38.

[42] L. Ai, Y. Zhou, J. Jiang, Removal of methylene blue from aqueous solution by montmorillonite/CoFe$_2$O$_4$ composite with magnetic separation performance, Desalination, 266 (2011) 72–77.

[43] Z. Qin, P. Yuan, S. Yang, D. Liu, H. He, J. Zhu, Silylation of Al13-intercalated montmorillonite with trimethylchlorosilane and their adsorption for Orange II, Appl. Clay Sci., 99 (2014) 229–236.

[44] P. Demirçivi, Synthesis and characterization of Zr(IV) doped immobilized cross-linked chitosan/perlite composite for acid orange II adsorption, Int. J. Biol. Macromol., 118 (2018) 340–346.

[45] X. Jin, B. Yu, Z. Chen, J.M. Arocena, R.W. Thring, Adsorption of Orange II dye in aqueous solution onto surfactant-coated zeolite: characterization, kinetic and thermodynamic studies, J. Colloid Interface Sci., 435 (2014) 15–20.

[46] N.M. Mahmoodi, U. Sadeghi, A. Maleki, B. Hayati, F. Najafi, Synthesis of cationic polymeric adsorbent and dye removal isotherm, kinetic and thermodynamic, J. Ind. Eng. Chem., 20 (2014) 2745–2753.

[47] S. Yavari, N.M. Mahmodi, P. Teymouri, B. Shahmoradi, A. Maleki, Cobalt ferrite nanoparticles: preparation, characterization and anionic dye removal capability, J. Ind. Eng. Chem., 59 (2016) 320–329.

[48] H.N. Bhatti, A. Jabeen, M. Iqbal, S. Noreen, Z. Naseem, Adsorptive behavior of rice bran-based composites for malachite green dye: isotherm, kinetic and thermodynamic studies, J. Mol. Liq., 237 (2017) 322–333.

[49] A. Almasian, F. Najafi, M. Mirjalili, M.P. Gashti, G.C. Fard, Zwitter ionic modification of cobalt-ferrite nanofiber for the removal of anionic and cationic dyes, J. Ind. Eng. Chem., 67 (2016) 306–317.

[50] L. Sellaoui, G.L. Dotto, S. Wjihi, J.O. Gonçalves, L.A.A. Pinto, A.B. Lamine, A. Erto, Thermodynamic analysis of single and binary adsorption of Food Yellow 4 and Food Blue 2 on CC-chitosan: application of statistical physics and IAST models, J. Mol. Liq., 232 (2017) 499–505.

[51] A. Maleki, U. Hamesadeghi, H. Daraei, B. Hayati, F. Najafi, G. McKay, R. Rezaee, Amine functionalized multi-walled carbon nanotubes: single and binary systems for high capacity dye removal, Chem. Eng. J., 313 (2017) 826–835.

[52] H. Mansouri, R.J. Carmona, A. Gomis-Berenguer, S. Souissi-Najar, A. Ouederni, C.O. Ania, Competitive adsorption of ibuprofen and amoxicillin mixtures from aqueous solution on activated carbons, J. Colloid Interface Sci., 449 (2015) 252–260.

[53] C. Muthukumaran, V.M. Sivakumar, M. Thirumarimurugan, Adsorption isotherms and kinetic studies of crystal violet dye removal from aqueous solution using surfactant modified magnetic nanoadsorbent, J. Taiwan Inst. Chem. Eng., 63 (2016) 354–362.

[54] J.Y. Song, S.H. Jhung, Adsorption of pharmaceuticals and personal care products over metal-organic frameworks functionalized with hydroxyl groups: quantitative analyses of H-bonding in adsorption, Chem. Eng. J., 322 (2017) 366–374.

[55] C.R. Minitha, M. Lalitha, Y.L. Jeyachandran, L. Senthilkumar, R.T.R. Kumar, Adsorption behaviour of reduced graphene oxide towards cationic and anionic dyes: co-action of electrostatic and $\pi - \pi$ interactions, Mater. Chem. Phys., 194 (2017) 243–252.

[56] K. Samal, C. Das, K. Mohanty, Eco-friendly biosurfactant saponin for the solubilization of cationic and anionic dyes in aqueous system, Dyes Pigm., 140 (2017) 100–108.

[57] X.J. Yue, J.X. Li, T. Zhang, F.X. Qiu, D.Y. Yang, M.W. Xue, Ultralong MnO_2 nanowires enhanced multi-wall carbon nanotubes hybrid membrane with underwater superoleophobicity for efficient oil-in-water emulsions separation, Ind. Eng. Chem. Res., 57 (2018) 10439–10447.